Proceedings of Global Power and Propulsion Society
ISSN-Nr: 2504-4400
GPPS Xi'an21
18th – 20th October, 2021
www.gpps.global

GPPS-TC-2021-0109

Study on the Flow Characteristics of Fan Coupled Nacelle Intake under Different Angle of Attack

Min Qi
Northwestern Polytechnical University
qimin111@formail.com
Xi'an, Shannxi, China

Zhanxue Wang
Northwestern Polytechnical University
wangzx@nwpu.edu.cn
Xi'an, Shannxi, China

Li Zhou
Northwestern Polytechnical University
zhouli@nwpu.edu.cn
Xi'an, Shannxi, China

Wenjian Deng
Northwestern Polytechnical University
dengwenjian@nwpu.edu.cn
Xi'an, Shannxi, China

ABSTRACT

The main function of nacelle intake is to provide the fan with stable and uniform flow in a wide operating range. The next-generation civil turbofan engine requires nacelle intake to have shorter length and larger lip thickness. However, the thicker lip is, the higher the probability flow to be separated, and the total pressure distortion disturbance is quickly transmitted to the fan, which causes the increase of the inhalation of distortion. Eventually, the stability of the engine is destroyed. Therefore, it is necessary to study the distortion of the nacelle intake and the coupling effect of the nacelle intake and fan. Aiming at the coupling effect of intake distortion of the nacelle intake and fan under a high angle of attack, the research focus on the flow characteristics of isolated nacelle intake and intake/ fan integrated model under different angle of attack. Results show that the intake presents different flow patterns under different Ma and mass flow rate; however, the interaction between the intake and fan presents a similar pattern. The presence of fan leads to the flow swirl angle changes significantly and mass redistribution. The studies also indicate that the intake distortion sensitivity level decrease with the fan coupling. The sensitivity of the distortion index decreases from 4.057% to 0.315% under cruise condition; the sensitivity of the distortion index decreases from 0.186% to 0.1423% under take-off condition..

Key words: Numerical Simulation, Nacelle Intake, Angle of Attack, Fan Coupling

INTRODUCTION

Nacelle intake is an essential part of aero-engine, the main function of intake is to provide the fan with stable and uniform flow in a wide operating range. When the propulsion system is operating, distortion flow happens on the fan surface. During cruise, the work condition for fan is stable and the intake distortion is low. However, under harsh environment conditions such as take-off(/cross wide), the angle of attack(AOA) increases which induces flow separated, high pressure and temperature distortion happen at the fan surface, which may cause decreasing of the engine surge margin and increasing of fuel consumption, furthermore, the stability of the engine will be destroyed. The nacelle intake is not a separate working entity out of bag of propulsion system, it should be designed and evaluated from the perspective of needs of propulsion system. The nacelle intake and fan are closely connected in structure, highly coupled in performance. Compared with other destabilizing factors that affect engine operation, intake distortion has the most obvious adverse effect on fan/compressor stability margin (Liu Daxiang et al, 2004. Lian Xiaochun et al, 2005. Li Zhengneng, 2006. Zhao Haigang et al, 2010). The next generation civil turbofan engine requires nacelle intake has a shorter intake length and larger lip thickness. However, the thicker lip is, the higher probability flow to be separated, and the total pressure or distortion disturbance is quickly transmitted to the fan due to shorter intake length, which causes the increasing of inhalation of ground vortices and distortion during flight at high attack of angle. Therefore, it is necessary to study the distortion of the nacelle intake and its influence and their coupling effect.

Hodder and Motycka first observed the stabilizing effect of the fan on the distortion level when the separation occurs(Hodder et al, 1982). Fidalgo conducted a flow deformation with an entire NASA rotor fan (Fidalgo et al, 2012).

The research is similar to the results from Hodder that the fan redistributes the mass flow in the area where the distortion occurs and generates greater tension. Stefan Kenneyused the rotor frozen model to simultaneously investigate the performance of the intake and the separation flow topology in the intake, which is in agreement with the experiment results(Stefan et al, 2014). Due to the high cost of a full-dimensional numerical simulation of fan, so far, researchers have used various simplified methods to study the coupling effect between intake and fan. The report(European Institute for Space Research, 2016) released by the European Institute for Space Research includes a study of the difference between the coupled model and isolated nacelle model, and replace the fan by the rotor disk model and the body force model to study the difference of variant simplified models. Yunfei Ma proposed a hybrid fidelity method, which uses IBMSG to express the effect of the fan, and studied various test cases(Ma Y., 2018). Wang cheng from Nanjing University of Aeronautics and Astronautics studied the development of ground vortices after adding a real propeller blades behind the intake(Cheng Wang, 2018). Xu Zhulin of the China Aerodynamics Research and Development Center researched the method of embedding the body force model block in the intake model(Zhulin Xu, 2019). This processing method makes the body force modeling and integrated calculation easier and faster.

Most of related publications on coupling effect of nacelle intake and the fan/compressor use simplified methods. In this work, the isolated nacelle intake and nacelle intake/fan integrated system is taken as the research object, the flow characteristics of isolated nacelle intake and nacelle intake/ fan integrated model are studied. The mechanism of nacelle intake distortion under different angles of attack are explored and the influence discipline on the performance of the nacelle intake from the fan is acquired.

GEOMETRIC MODEL AND NUMERICAL METHODOLOGY

Geometric model

The isolated nacelle intake model, shown in Figure 1, is consisted of nacelle cowl, lip, intake and spinner when omitting the effect of the pylon, wing and exhaust system; fan model, shown in Figure 2, is consisted of rotor blades and stator blades. Because the left and right parts of nacelle are symmetrical, the fan have periodicity. So the nacelle / fan couple model, shown below, is consisted of isolated nacelle, spinner, fan rotor blade and stator blade. Nacelle / fan couple model, shown in Figure 3, is consisted of isolated nacelle, spinner, fan rotor blade and stator blade. The key design parameters are shown in the table 1.

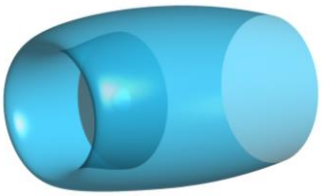

Figure 1 Nacelle model

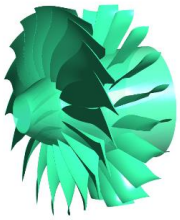

Figure 2 Fan model

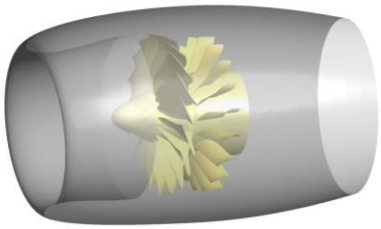

Figure 3 Nacelle intake and fan couple model

Table 1 key design parameters

Parameters	Values
Intake length/mm	300
Highlight diameter/mm	500
Highlight aspect ratio	1.02
Droop angle/（°）	4°
Radial offset/mm	25
Fan diameter/mm	498
Passage number	18
Corrected speed /rpm	18268
Corrected mass rate Kg/s	34

Numerical simulation methodology

The numerical simulations use ANSYS CFX software. The equations solved were the fully 3D, steady, compressible, Reynolds-average Navier-Storks equations. Stand $k-\varepsilon$ model was chosen as the turbulent model, the convection term, turbulent kinetic energy k and turbulent energy dissipation ε in the flow equation all adopt the second-order upwind roe flux splitting scheme, the turbulent model adopts the standard model, the wall is the standard wall function, and the fluid is ideal gas. The frozen rotor interface model was applied as it's better suited to separated flows.

Boundary condition settings of the computational domain are presented in Figure 4. The far-field is 15 times of the nacelle diameter wide and 15 times of the nacelle length. Velocity inlet condition was applied to the free-stream flow inlet, of which the static temperature, and flow Mach number are given. The pressure outlet condition is applied of the far-field outlet, of which the static temperature is given. The target mass flow rate outlet condition is given at the fan outlet. The Cartesian velocity component and static pressure and static temperature are given as initializations. For both cruise and take-off conditions, a range of 0-20 degrees of angle of attack are considered as variable, and is taken as value at every interval of 5 degree. For the model studied in current work, the structured grid was generated by ICEM software, the grid near the nacelle wall and blade were densified with the first cell height of approximate $10 < y^+ < 300$. Details of the full 3D computational domain are presented in Figure 4. 14~20 million nodes grids were used to verify the grid independence. When the grids reach 17 million, the total pressure recovery coefficient changes with the grid does not exceed 1%. Therefore, the selection of 6 million grids of nacelle intake and 11 million grids of the fan blades calculation have reached the requirement of grid independent.

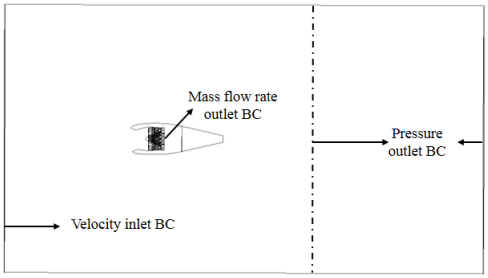

Figure 4 Boundary condition settings

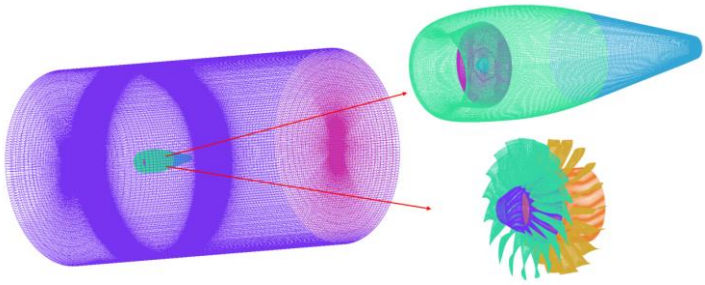

Figure 5 Grid of nacelle intake and fan blades

Performance parameter definition

In order to compare and evaluate the performance of the intake under different angle of attack. The total pressure recovery coefficient σ_i , the distortion index DC_{60} are used to evaluate the performance of the nacelle intake. The pressure ratio π^* and efficiency η are used to evaluate the performance of fan.

RESULTS AND DISCUSSION

Numerical simulation validation

In order to verify the accuracy of the numerical method. The ARA experimental model of cowl1 was used, the calculation model was determined according to the dimensional data(Shaohua Hei, 2017). The three-dimensional model of nacelle is shown in figure 4. Numerical calculations are carried out under the same boundary conditions, the simulation data of nacelle wall pressure distribution were obtained to compare with the experimental data, which is shown in figure 5. Where is the ratio of wall static pressure to the incoming flow total pressure, and the X/D_MAX is the ratio of axial position to the maximum diameter of nacelle. It can be seen that the simulation data is basically consistent with the experiment values, thus, the stand model can be well used to predict the flow in the nacelle intake.

Figure 6 Schematic diagram of nacelle

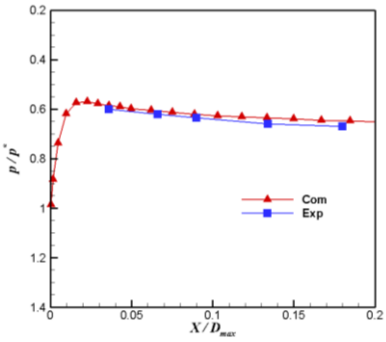

Figure 7 Comparison of the calculation and experiment

Flow features of the isolated nacelle intake under cruise condition.

To better understand the effect of the fan on the intake and explore the interaction mechanism, the isolated nacelle intake flow feature under different AOA was studied first. Figure 8 shows the contour of Ma distribution on symmetry plane. Since nacelle has a droop angle of 4°, when AOA is 5°, flow passage along the intake is proximately symmetry, the degree of the flow passage contraction is similar, the flow field of the upper and lower intake is not much different. With the further increase of AOA, the stagnation point of the upper lip moves inward, a large high speed and low pressure zone is gradually formed on the cowl. On the contrary, the stagnation point on the lower lip moves outward along the cowl, flow

detour along the lip is more intensive, the pressure gradient increases, an obvious high-speed zone is formed at the throat. Furthermore, separation appears when AOA reaches 20°. With the further increase of AOA, the speed gradually approaches the speed of sound, the position of the aerodynamic throat is forced to move forward, finally flow separates under a larger reverse pressure gradient.

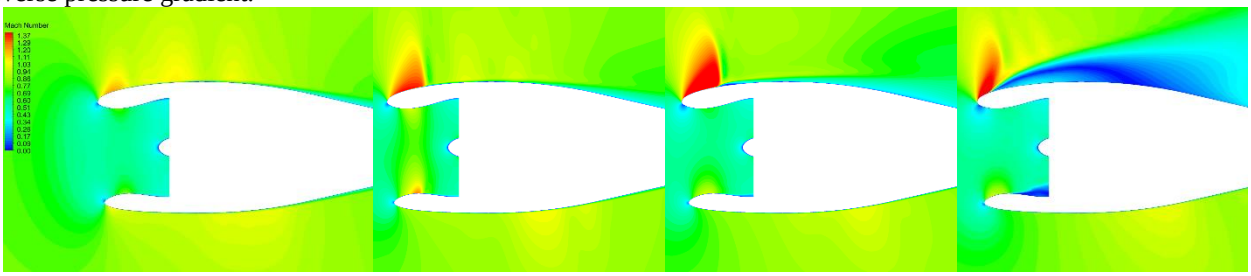

Figure 8 Ma contour on the symmetry plane of the isolated nacelle intake under cruise

When the intake is operating under the working condition with AOA, the velocity above and below the centerline have evident gap, and a pressure difference will be formed on the fanface. If the AOA was too large, the pressure on the lower surface of the intake will be further reduced, and the pressure gradient in the diffuser will continually increase, meanwhile due to the ununiformed circumferential pressure distribution, the lower part of the fanface has the lowest pressure, driven by the pressure gap on the side part, cross flow is induced, thus a pair of counter vortex appears, finally a recirculation zone will be formed below the intake. Figure 9 shows the total pressure recovery coefficient distribution on the Aerodynamic Interface Plane (AIP) of the nacelle intake under different angles of attack during cruise. It can be seen that there is an ultra-low total pressure recovery zone around the wall at any AOA, which is due to the high pressure gradient along the diffuser. In the intake, as the increasing of AOA, the flow above the centerline becomes more and more gentle, the acceleration of the flow around the lip below the centerline gradually increases. As the incoming flow slopes downwards, the expansion degree of the diffuser below the centerline becomes relatively large, the pressure gradient becomes high, and the thickness of the boundary layer gradually becomes thicker, the high-pressure zone gradually moves upward, and an obvious low-pressure zone is formed on the lower wall at AIP. Meanwhile, it is obvious that when the AOA arrives 5°, the distribution of the total pressure recovery coefficient on the AIP is the most uniform along the circumferential direction.

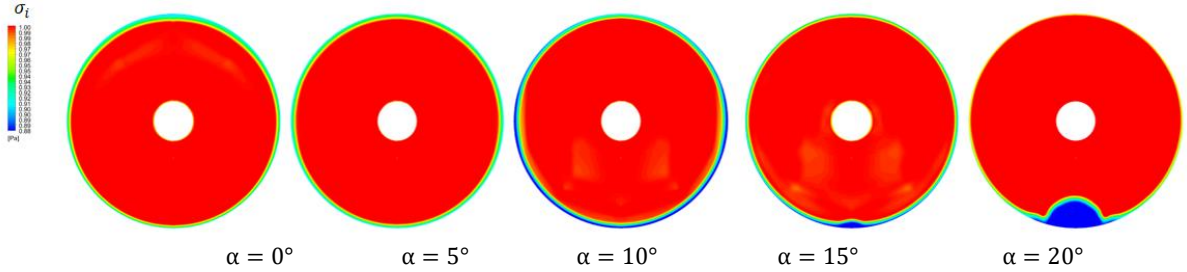

Figure 9 Total pressure recovery coefficient distribution on AIP of isolated nacelle intake under cruise

Figure 10 shows the trends of isolated nacelle intake performance with the AOA in cruising. It can be seen that as the AOA increases, the total pressure recovery coefficient decreases, and the distortion index gradually increases. Both the total pressure recovery coefficient and distortion index reached the best values when the AOA is 5°. In summary, the important feature of intake flow under high angel of attack is the possible separation within the lip and it only occurs at the lip on the windward. Under the condition of AOA, even if the mass flow rate is less than 1, the stagnation point on the windward of the nacelle is outside the lip. Flow accelerates from the stagnation point around the lip, and then decelerates sharply due to the counter pressure gradient, eventually may causing the separation of flow in the boundary layer and nacelle intake performance drops sharply.

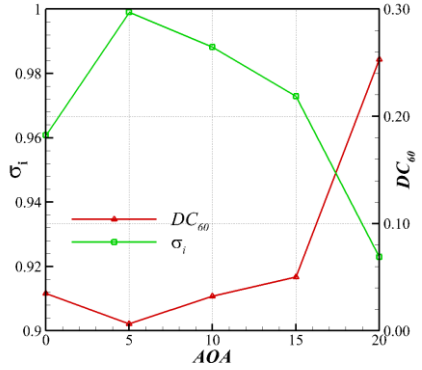

Figure 10 Performance of the isolated nacelle intake vary with the AOA under cruise

Flow features of the fan coupled nacelle intake under cruise.

The performance of fan coupled intake and fan under cruise at different AOA is showed in figure 11. The isolated nacelle intake and fan coupled intake performance show different trend. For the isolated intake, the total pressure recovery coefficient and distortion index reaches the best values when the AOA is 5°, while for the fan coupled intake, the total pressure recovery coefficient and distortion index reaches the best values when the AOA is 10°. Also, fan performance reaches the best value when AOA is 10°. The change rate of the total pressure recovery coefficient of isolated intake does not exceed 0.999%, the maximum change rate of the distortion index is 4.057%, the change rate of the total pressure recovery coefficient of the fan-coupled intake does not exceed 0.337%, and the maximum change rate of the distortion index is 0.315%. Here the change rate refers to the amount of change of the corresponding parameter for each degree change of angle of attack. Comparing the performance between fan coupled intake and isolated nacelle intake, which shows that the nacelle intake performance has improved with higher average total pressure recovery coefficient and lower distortion index throughout the changing range of high AOA; the performance of the fan coupled intake shows relative hysteresis, which can tolerate a higher angle of attack. Also, fan total pressure rise and efficiency changes along with the intake performance, reaches the best value when AOA is 10°.

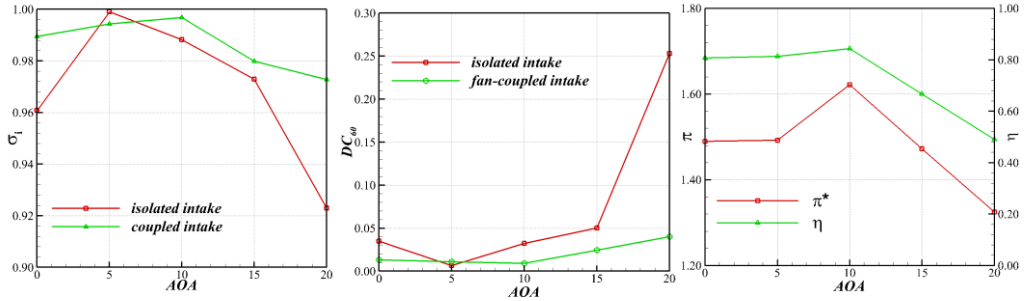

a) Total pressure recovery coefficient b) Distortion index c) Total pressure ratio and efficiency

Figure.11 Nacelle intake and fan performance under different AOA at cruise

Figure 12 a) shows the pressure distribution and streamline along the nacelle intake of isolated intake and fan coupled intake at 20° AOA. It can be seen that from the highlight section to the fanface, the radial pressure difference changes significantly. In the first cross section, as the incoming upwash flow continues to tilt, the low-pressure area gradually moves from the upper wall to the lower wall; The second cross section is located at the beginning of the diffuser, where the distribution is relatively uniform; The third cross section is located at AIP, where flow is fully decelerated and pressurized in the diffuser. As the flow below the centerline is accelerated around the lip severely, the reverse pressure gradient is larger, and the pressure loss is larger, causing the upper face pressure is higher, while the lower face pressure is lower at AIP. As a consequence, the distortion level increases. Figure 12 b) shows the streamline distribution, for the isolated intake, the lower pressure is the lowest. Under the pressure of the lateral pressure difference, a pair of counter vortices with opposite rotation directions are formed directly below the plane. The role of fan blades is to rotate to suck and spin the flow especially flow at shroud due to the high line speed. Affected by suction, flow is accelerated in the intake and the inlet flow pressure gap gets bigger at the first cross section, and this suction effect deficits along the intake. Meanwhile, this acceleration will suppress the separation at high angle of attack. Affected by the counterclockwise rotate of fan, the streamline on AIP obviously move towards counterclockwise direction, and weaker lateral flow is formed. Also, affected by acceleration, mass flow is redistributed, for the isolated intake, most flow mass goes to the upper face, while for the coupled intake, mass flow cross the lower face increase.

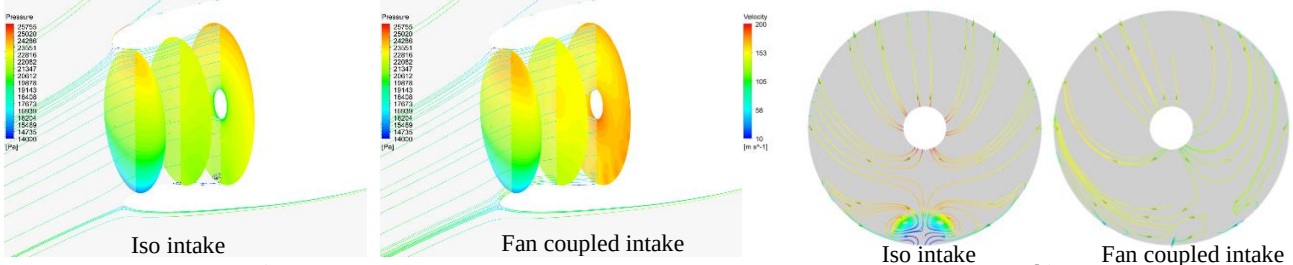

a) b)

Figure 12 Isolated intake and fan coupled intake comparison under cruise condition

Figure 13 shows the total pressure distribution along the circumferential direction on AIP of both intake under different angles of attack during cruise. It can be seen that the average total pressure level of fan-coupled intake is higher, and the total pressure distribution is more uniform, especially at high AOA. Similar to the isolated intake, as the increase of AOA, there is a low total pressure zone on the lower zone of the fan coupled intake, difference is the range of the low pressure

zone around the wall is reduced. Also, it can be seen that when AOA is 10°, the total pressure distribution of fan coupled intake is the most evenly.

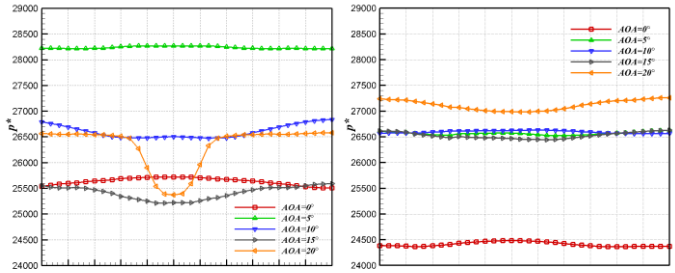

a) Isolated intake b) Coupled intake

Figure.13 Total pressure circumferential distribution under cruise

As streamlines on the fan face change, the velocity and the pressure redistribute, resulting in circumferential side flow, which will induce tangential component. The inlet relative flow angle should keep constant to satisfy the blade incidence. While due to the asymmetry of the nacelle intake itself, when the angle of attack is low, incoming flow to the fan is not uniform, the annulus distribution is uneven. Figure 14 shows the relative flow angle β_1and Ma blade-to-blade contours at three different span location (10%, 50%, 90%). As can be seen from the figure, a low relative flow angle region exits at any cases which indicates the circumferential unevenness of fan flow, for the three different location, the shroud region encounters a relative higher relative flow angle, and the hub region encounters a relative lower relative flow angle

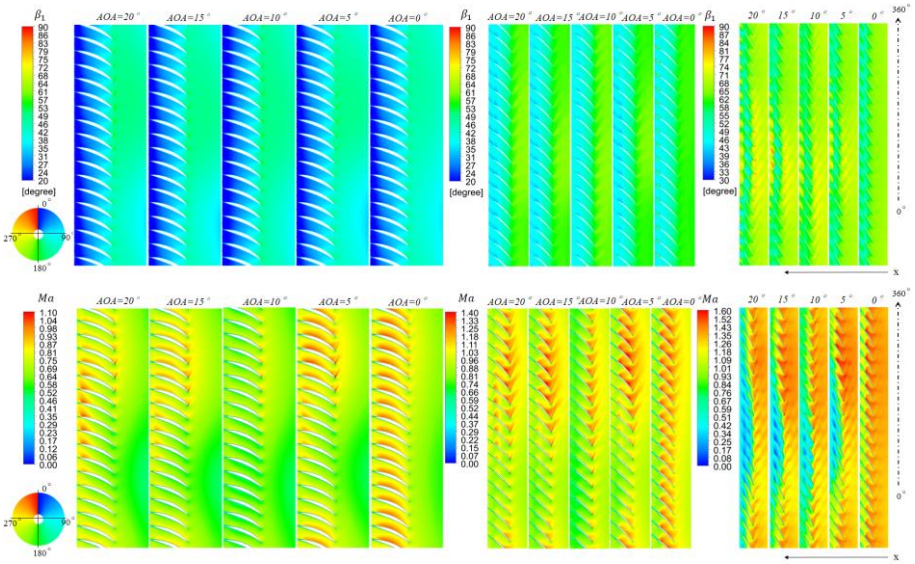

10% 50% 90%

Figure 14 blade to blade absolute flow angle and Ma distribution on differetn normalized span

The contour also shows that even though the blade is working at a lower relative flow angle at 0° AOA, it is not the optimal incidence for blades. The Ma contour shows that with the increase of AOA, the incoming flow incidence of fan gradually changes from a negative angle to a positive angle of attack. Both negative angle and positive angle is not benefit for the fan performance. At a negative incidence(low relative flow angle), the acceleration around the leading edge will cause flow loss increase, even causing a shock-wave at the leading edge at suction face, as shown in the 10% span Ma contour. At a positive incidence, separation is more likely to be happen due to the viscous effect of boundary layer at the suction face, for most cases, the shroud is not operating at an ideal condition as shown in the 90% span Ma contour. When flow separate, the shove wave-boundary layer interaction will cause flow losses increase rapidly, more than this, the cascade wake loss will increase, the gap between wake and main-flow increase, and the mixing loss increase. As can be seen, at 10% and 50% span, the passage flow is the most ideal when AOA reaches 10°. Also, as state above, the region near the hub as well as the shroud change significantly with the increase of AOA, this causes form the low-energy flow from the intake. Which, mainly in the boundary layer flow around the intake wall and spinner wall, also, as analyzed above, is easily affected by changes in AOA. The pressure distortion is transmitted along the fan blade. Since the low-energy flow's compressibility is higher, the pressure rise is higher. However, there is an imbalance between the pressure-rise and heat transfer across the fan blades, the pressure loss is also higher, the fan efficiency is not ideal. In order to explore the interaction mechanism between the intake and fan, swirl angle at AIP is extract and shown in figure 15. The swirl angle is defined as the angle between circumferential and axial velocity components(Mehdi, 2014), compare to the velocity triangle

above, it is clear that the swirl angle changes opposite with the relative flow angle, when the relative flow angle increase, the swirl angle decrease. As shown in figure 18, the near hub region has the highest level of swirl angle while the near cascade region has the lowest level, which is contrary to figure 15, this also means that the relative flow angle distortion can be represented by studying the swirl angle distortion on AIP.

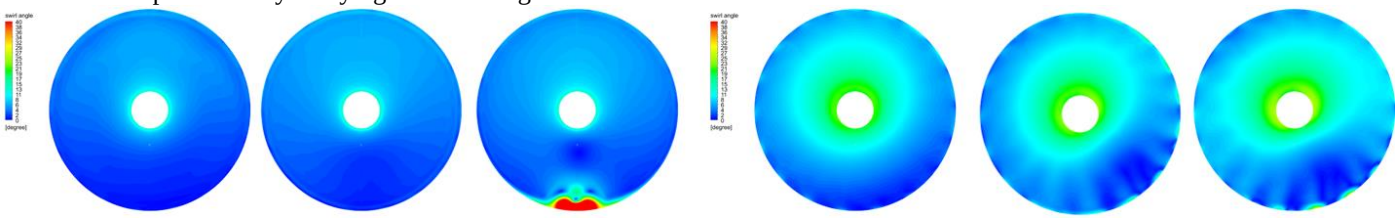

α=0° α=10° α=20° α=0° α=10° α=20°

a) Iso intake Fan coupled intake

Figure 15 Velocity angle contour on the inlet face of fan at cruise

The contour also shows that the swirl angle for isolated intake is much lower, as separation occurs, a counter swirl appears at the lower face. For the fan coupled intake, the average swirl angle level is much higher with a corrugated shape. The same changing trend mainly located at the lower face, as the swirl angle at lower face increase with the increase of AOA. Also, the banded relative higher swirl angle region around annulus appears with the increase of AOA. To evaluate the swirl distortion level, the bulk swirl intensity $\overline{\tau}_{87}$, counter swirl intensity($\overline{\tau}_{87\max} - \overline{\tau}_{87\min}$)/2, bulk swirl index SCB and counter swirl index SCT are calculated and shown as figure 16 and 17. This four swirl distortion is proposed by Peng Chengyi, and is able to accurately assess the intensity and structure of typical swirl flows by numerical simulation calculations and wind tunnels(Peng Chengyi, 1994). For pure bulk swirl, the bulk swirl index SCB is 1, and the counter swirl index SCT is 0; for pure counter swirl, the bulk swirl index SCB is 0 and counter swirl index SCT is 1. By applying the swirl evaluation index, it can be seen from the figure that for both isolated and coupled intake, the intensity of bulk swirl and counter swirl gradually increase with the change of AOA, which indicates that the swirl distortion increase with AOA. Also, the bulk swirl intensity is stronger than the counter swirl intensity, the intensity of both swirl structure is larger than that of isolated intake. While with the increase of AOA, the bulk swirl index decrease, the counter swirl index increase, especially for the coupled intake, which is consistent with the analyzed above. For coupled intake, bulk swirl index is much larger than counter swirl, that means the flow field is dominated by the overall vortex with certain direction, and there is small local vortex in the flow. For the isolated intake, when AOA reaches 20°, the bulk swirl index and counter swirl index are both around 0.5, which means there is a local vortex in the flow field, and the vortex core is not at the center of the section.

In order to more intuitively display the swirl angle distortion on the interface, swirl angle is normalized as below:

$$D_{1(\text{angle})} = \frac{v_{angle-\max} - v_{angle-\min}}{v_{angle-av}} \qquad (1)$$

And the relationship of this parameter varies with the AOA are shown in figure 20. It can be seen that for isolated intake, the changing trend of swirl angle distortion is consistent with the changing trend of intake total pressure recovery, for coupled intake, the swirl angle distortion is consistent with the changing trend of intake total pressure recovery fan efficiency.

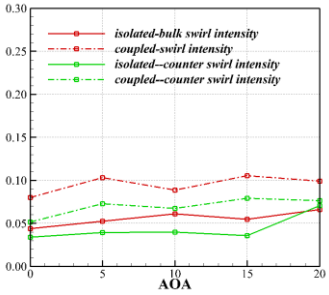

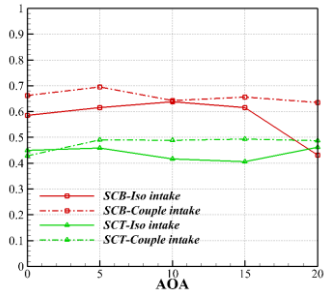

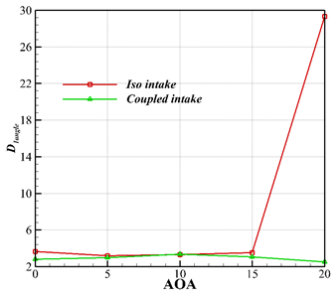

Figure 16 Swirl distortion intensity **Figure 17 Swirl distortion index** **Figure 18 Swirl angle distortion**

In summary, as the fan redistributes the flow of the intake, the performance of the intake is significantly improved with better total pressure recovery and lower distortion, most of all, the intake is able to working at higher angle of attack without separation in the intake. In addition to the pressure distortion on fanface, the swirl angle at the interface of intake and fan also changes significantly, and the performance of the fan changes accordingly.

CONCLUSIONS

In this paper, the performance and flow characteristics of isolated nacelle intake and nacelle intake coupled with fan under different angle of attack at both cruise and take-off conditions are studied. The distortion of the nacelle intake and

its influence on the fan and the coupling effect of the nacelle intake and fan when operating under different angle of attack is obtained as follow:

1. Under cruise condition, with the increase of angle of attack, the total pressure recovery coefficient of isolated intake fist increases then decreases, and the distortion index changes the opposite. Both the total pressure recovery coefficient and the distortion index reach the optimal values when the incidence is 5°.
2. The performance of fan coupled intake have different trends compared to isolated intake.Compared with isolated intake, the fan coupled intake the performance of the intake has been improved with higher total pressure recovery coefficient and lower pressure distortion index. Also, the intake is able to tolerant higher angle of attack without separation in the intake. In addition, the changing trend of swirl angle distortion vary with angle of attack is consistent with the changing trend of fan total pressure ratio and fan efficiency.
3. The existence of fan coupled to the intake decreases the sensitivity of the intake distortion level when operating under angle of attack condition. Under cruise, the sensitivity of distortion index decreases from 4.057% to 0.315%, and the sensitivity of swirl angle distortion decreases from 5.201 to 17.245%.

NOMENCLATURE

σ_i	=	Total pressure recovery coefficient
DC_{60}	=	Total pressure distortion index
π^*	=	Fan pressure ratio
η	=	Fan efficiency
AOA	=	Anggle of attack
AIP	=	Aerodynamic interface plane
P*	=	Total pressure, Pa
β_1	=	Relative flow angle, degree
$\overline{\tau}_{87}$	=	Buik swirl intensity
SCB	=	Bulk swirl index
SCT	=	Counter swirl index

REFERENCES

[1] Daxiang Liu, Peiliang Ye Peiliang, Jun Hu. (2004) *Guidelines for the Stability Design and Evaluation of Aviation Gas Turbine Engines*. Aviation Industry Press.

[2] Zhengneng Li. (2006). *Aircraft Compo-nents and System Desig*. Beijing University of Aeronautics and Astronautics Press.

[3] Xiaochun Lian, Hu Wu. (2005), *Principles of Aero Engine*s.. Northwestern Polytechnical Uni-versity Press.

[4] Haigang Zhao, Jiyun Qu, Jianbang Shi. (2010). Filghtting Test of Inlet/Engine Compatibility During Rapidly Changing Aircraft Maneuvers. *Journal of Aerospace ower*. 25(9). pp. 2077-2082.

[5] Hodder and Stoughton. (1982). The Functions and Operations of a Specialty. T*he British Journal of Psychiatry*. 140(4):446-446.

[6] Fidalgo, V.J, Hall C and Cloin Y. (2012). A study of fan-distortion interaction Within the NASA Rotor 67 Transonic Stage *ASME J. Turbomach*. 134(5). p.051011.

[7] Stefan Kennedy. (2014). Computational Investigation of Inlet Distortion at High Angles of Attack. *Journal of Aircraft*. Vol. 51, No. 2.

[8] European Space Institute. (2016). *A Review of Inlet-Fan Coupling Methodologies*.

[9] Ma Y., Cui J., Vadlamani N.R. (2018). Effect of Fan on Inlet Distortion: A Mixed Fidelity Approach. *AIAA Journal*, 56(6):2350-2360.

[10] Cheng Wang, Bo Li. (2018). Numerical Simulation of Ground Vortex in Nacelle Inlet with Fan Blades. *Journal of Chongqing Institute of Technology*. v.32:No.384-(07):105-114.

[11] Zhulin Xu, Xingya Da. (2019). Computational Study on S-Shaped Inlet and Fan Coupling Based on Body Force Model. *Journal of Propulsion Technology*, (7). pp. 1441-1448.

[12] Zhulin Xu, Xingya Da. (2019). A Body Force Model for the Computation of Inlet and Fan Intergration. *Journal of Propulsion Technology*. 40(04):18-26.

[13] Shaohua Hei, Shenglan Jiang. (2017). Numerical Simulation on Nacelle Drag of Turbofan Engine with a Large Bypass Ratio. *Journal of Shenyang Aerospace ace University*. 34(4):48-54.

[14] Mehdi, Ahad. (2014). *Effect of swirl distortion on gas turbine operability.* Cambridege University.

[15] Chengyi Peng, Jiaju Ma, Junfei Yin. (1994). Measurement of Inlet Swirl in Flight. *Journal of Propulsion Technology*. (4):8.